C−S and C−H Bond Activation of Thiophene by Cp*Rh(PMe_3): A DFT Theoretical Investigation

Andrew L. Sargent* and Emily P. Titus[†]

Department of Chemistry, East Carolina University, Greenville, North Carolina 27858

Received July 10, 1997[⊗]

A theoretical analysis of the C−S and C−H bond-activation pathways involving thiophene and Cp*Rh(PMe_3) is presented in which B3LYP density-functional theory is utilized. In addition to the traditional pathway which connects the η^2-coordinated intermediate with the C−H bond activation products, a new pathway is discussed which connects the η^1 S-bound intermediate with these products. Calculations are performed in the basis of molecular orbitals of the interacting fragments for the reactive η^1- and η^2-coordinated intermediates to examine the orbital interactions and density transfer between the fragments. The calculated binding energy of the η^1-coordinated intermediate is 15.5 kcal/mol weaker than that for the η^2-coordinated intermediate due to the increased energy separation and reduced density transfer between the molecular orbitals of the interacting fragments. The structure of the transition state connecting the η^1-coordinated intermediate with the C−S bond-activated product involves the strong overlap of the HOMO of the metal fragment with the LUMO of thiophene which results in the close proximity of the distal carbons on thiophene with the methyl groups of the Cp* ligand. Substitution of bulky groups at the 3 and 4 positions on thiophene may result in a significant steric component to the C−S activation barrier. Substitution of bulky groups on all carbons results in a significant thermodynamic component to the instability of the ring-opened product. Preliminary results indicate that the lack of reactivity toward C−S bond activation in Cp*Re$(CO)_2$ is due to the participation of the electron withdrawing carbonyl groups in the transfer of density between the interacting fragments.

Introduction

Catalytic hydrodesulfurization (HDS) is a step in industrial oil refining in which sulfur-containing organic compounds are removed from crude oil by their chemical conversion to H_2S and hydrocarbon products.[1] Implicit in this process are two important and fundamental chemical reactions: the initial coordination of the sulfur compound to the metal complex and the cleavage, or activation, of the carbon−sulfur bonds. Much of what is known about the chemistry of C−S bond activation comes from recent model studies involving homogeneous transition-metal organometallic complexes,[2] since the complicated nature of the heterogeneous catalyst used in industry precludes its investigation with the usual chemical diagnostic techniques.[3] In the model studies, thiophene is the most widely investigated organosulfur substrate due, in part, to the difficulty associated with its desulfurization in the HDS process. While there is some disagreement over the transferability of knowledge gained from the model studies to the actual industrial process, research activity in this area has blossomed since about 1990 and has led to an increased understanding of C−S bond-activation chemistry.[2]

Despite these recent advances, however, many aspects of the mechanism of C−S bond activation remain unclear. Contributing to this uncertainty is the subtle and diverse coordination chemistry of thiophene. Thiophene is known to coordinate single transition-metal centers in a variety of ways, including the sulfur-bound η^1 mode, the η^2 and η^4 modes which coordinate the metal via one and two carbon−carbon double bonds, respectively, and the η^5 coordination mode, which binds the metal through all five atoms of the ring.[4] All of these have been implicated as important intermediates in C−S activation reactions, yet recent model studies have indicated that only the η^1-coordinated intermediate directly inserts the metal into the carbon−sulfur bond and that pathways connecting the π-coordinated complexes to the ring-opened metallacycle first rearrange to the σ-coordinated η^1 complex.[5]

The importance of the η^1 coordination mode to the C−S bond activation of thiophene led us to investigate the electronic factors governing the relatively weak coordination strength of this binding mode.[6] Our analy-

[†] American Chemical Society−Petroleum Research Fund Scholar.
[⊗] Abstract published in *Advance ACS Abstracts,* December 15, 1997.

(1) Gates, B. C.; Katzer, J. R.; Schuit, G. C. A. *Chemistry of Catalytic Processes*; McGraw-Hill: New York, 1979, pp 390−477.

(2) For a recent review, see: Bianchini, C.; Meli, A. *J. Chem. Soc., Dalton Trans.* **1996**, 801−814.

(3) Markel, E. J.; Schrader, G. L.; Sauer, N. N.; Angelici, R. J. *J. Catal.* **1989**, *116*, 11−22. Bussell, M. E.; Somorjai, G. A. *J. Phys. Chem.* **1989**, *93*, 2009−2016. Friend, C. M.; Roberts, J. T. *Acc. Chem. Res.* **1988**, *21*, 394−400.

(4) Angelici, R. J. *Coord. Chem. Rev.* **1990**, *105*, 61−76.

(5) Dong, L.; Duckett, S. B.; Ohman, K. F.; Jones, W. D. *J. Am. Chem. Soc.* **1992**, *114*, 151−160.

S0276-7333(97)00585-2 CCC: $15.00
Publication on Web 01/05/1998

Scheme 1[5]

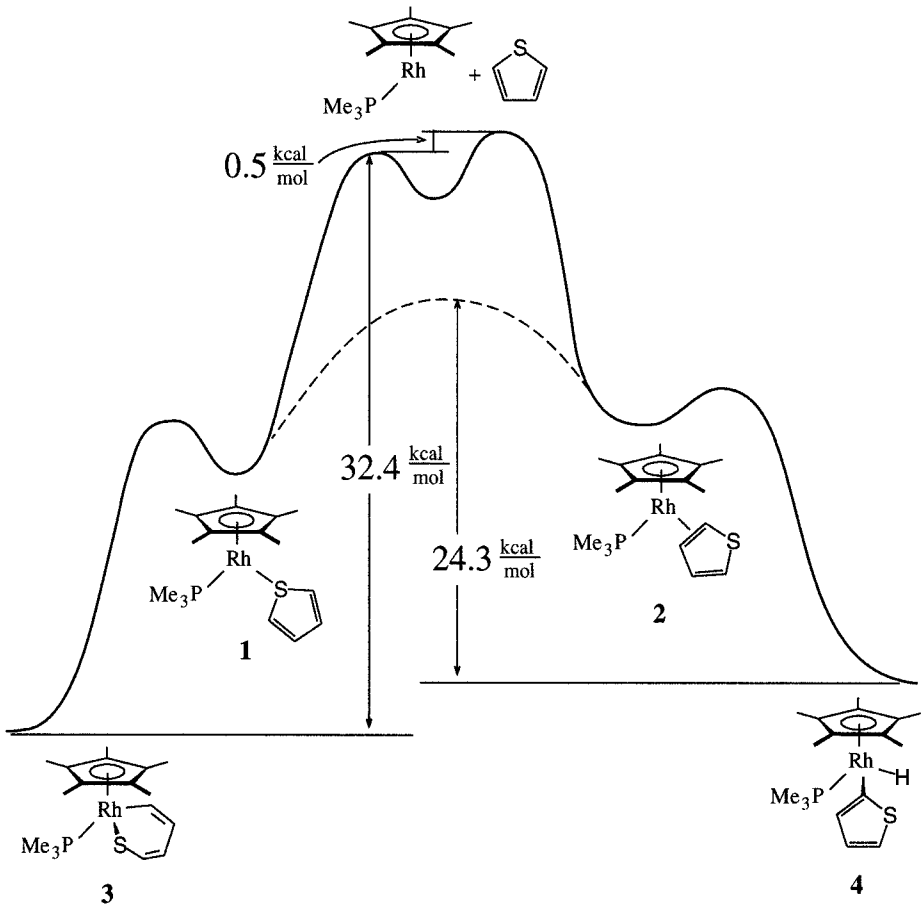

sis utilized approximate molecular orbital methods to compare the ligation aptitudes of η^1-coordinated thiophene and methyl sulfide ligands. Several other theoretical studies which have investigated the interaction between thiophene and metal species have been reported in the literature.[7,8] Some have examined complicated process occurring at metal sulfide surfaces[7a] or on metal sulfide clusters[7b,c] using simple models and low-level computational techniques (extended Hückel and Xα). Other studies have exploited the simplicity of the homogeneous model systems to investigate the nature[8a−d] and energetics[8e] of interactions between thiophene and single-metal organometallic complexes. These important studies have also utilized low-level techniques (Fenske−Hall, CNDO, and Xα), yet for the homogeneous model systems, higher levels of theory are feasible and could be applied to examine key components of the C−S bond-activation mechanism. In particular, higher levels of theory could be applied to determine the structures and relative energetics of reactive intermediates and transition states, quantities which are difficult or impossible to determine from experiment and which cannot be reliably determined at the lower levels of theory.

Herein lies the objective of the present study: to apply high-level theoretical techniques to a homogeneous HDS model system which has been well-characterized experimentally so that additional information can be obtained concerning the structures and energetics of transient species and the mechanisms associated with the bond-activation reactions. Such a system, in which thiophene interacts with the 16-electron metal complex Cp*Rh(PMe$_3$) (Cp* = η^5-pentamethylcyclopentadienyl), was recently reported by Jones and co-workers[5], and the results of the study are summarized in Scheme 1. The authors of the experimental study observed that the low-temperature reaction of the rhodium complex in the presence of thiophene led to the parallel formation of two products: the C−S bond activation product or ring-opened metallacycle (**3**) and the C−H bond activation product or 2-thienyl metal hydride (**4**). A variety of experiments including isotopic labeling studies led them to construct Scheme 1 to account for the parallel formation of the products.

The key components of this scheme are the η^1- and η^2-coordinated intermediates **1** and **2**, respectively, neither of which was directly observed in the experimental study. Other compounds which are not as reactive toward C−S or C−H bond activation have provided direct evidence for these coordination modes,[2] yet little is known about their relative stabilities or the mechanisms through which they react. One goal of the

(6) Sargent, A. L.; Titus, E. P.; Riordan, C. G.; Rheingold, A. L.; Ge, P. *Inorg. Chem.* **1996**, *35*, 7095−7101.

(7) (a) Zonnevylle, M. C.; Hoffman, R.; Harris, *S. Surf. Sci.* **1988**, *199*, 320−360. (b) Harris, S.; Chianelli, R. R. *J. Catal.* **1984**, *86*, 400−412. (c) Diemann, E.; Weber, Th.; Müller, A. *J. Catal.* **1994**, *148*, 288−303.

(8) (a) Sánchez-Delgado, R. A.; Herrera, V.; Rincón, L.; Andriollo, A.; Martín, G. *Organometallics* **1994**, *13*, 553−561. (b) Harris, S. *Organometallics* **1994**, *13*, 2628−2640. (c) Palmer, M.; Carter, K.; Harris, S. *Organometallics* **1997**, *16*, 2448−2459. (d) Blonski, C.; Myers, A. W.; Palmer, M.; Harris, S.; Jones, W. D. *Organometallics* **1997**, *16*, 3819−3827. (e) Rincón, L.; Terra, J.; Guenzburger, D; Sánchez-Delgado, R. A. *Organometallics* **1995**, *14*, 1292−1296.

present study is to more fully characterize **1** and **2** in this regard and to examine the proposed intramolecular rearrangement pathway which connects these intermediates (dashed line in Scheme 1).

The results are organized into several sections. Following a description of the theoretical methods, the η^1 coordination of thiophene is discussed. Results from the optimization of the molecular structure are examined from two perspectives. In the first, the orbital interactions between the Cp*Re(PMe$_3$) and SC_4H_4 molecular fragments are analyzed in detail with particular attention paid to the magnitude and direction of electron-density flow between the fragment molecular orbitals. The second approach also examines the electron-density transfer between the molecular fragments but avoids any ambiguity associated with the interpretation of results from a particular orbital model by analyzing the electron density directly in the form of deformation density plots. The η^1 coordination of tetramethylthiophene, which is highly resistant to C−S bond activation, is also examined in this section.

The next section focuses on the C−S bond-activation reaction which begins with **1** and results in the ring-opened product (**3**). Two approaches are taken to locate the transition state; a reaction coordinate calculation and a quadratic synchronous transit calculation, the former of which utilizes simple Hartree−Fock methods while the latter uses density-functional theory. The hypothetical ring-opened complex of tetramethylthiophene is also examined to assess the thermodynamic contribution to its lack of reactivity.

In the following three sections, the focus shifts to **2** and its subsequent reactivity. Fragment molecular orbital and difference density analyses are brought to bear on **2**. The direct rearrangement of **2** to **1** is examined through a quadratic synchronous transit calculation to obtain the transition state. Multiple aspects of the C−H bond-activation reaction of **2** are examined, including the rotational isomerization of the product (**4**) and a subsequent reductive-elimination reaction which yields **1**. These latter reactions provide an alternative intramolecular rearrangement pathway connecting products **4** and **3**, and viewed in reverse, they provide a pathway through which the C−H bond-activation products can be formed which *does not* include the η^2-coordinated intermediate (**2**).

The final section of the paper investigates some of the characteristics of other electron-deficient metal fragments in an attempt to correlate these characteristics with the fragment's propensity to undergo C−S bond activation. The metal fragments studied include (triphos)RhH (triphos = $CH_3C(CH_2PPh_2)_3$), $(PMe_3)_3IrCl$, Cp_2W, $(PEt_3)_2Pt$, and Cp*Re(CO)$_2$. Specific attention is paid to the last of these in an attempt to understand its lack of reactivity toward C−S bond activation.

Theoretical Details

Final equilibrium geometries were fully optimized in redundant internal coordinates[9] with density-functional theory (DFT) and a wave function incorporating Becke's three-parameter hybrid functional (B3)[10] along with the Lee−Yang−Parr correlation functional (LYP).[11] All calculations were performed with the GAUSSIAN 94 package.[12] Each equilibrium geometry was initially optimized at a lower level of theory corresponding to a restricted Hartree−Fock (RHF) wave function, a smaller basis set (vide infra), and nonredundant internal coordinates using a *z*-matrix specification. Partial geometry optimizations at this lower level served as the starting points for full optimizations in redundant internal coordinates at the DFT/B3LYP level.

Approximate transition state geometries were found via the QST2 or QST3 algorithms,[13] the latter of which utilized geometries from reaction coordinate calculations in nonredundant internal coordinates as the initial guess for the transition state structures. Due to the extreme CPU demand of the QST2 and QST3 calculations on a system the size of ours, the standard convergence thresholds for the maximum and root-mean-square displacements of the internal coordinates in the gradient calculations were relaxed from values of 0.0018 and 0.0012 Hartrees/Bohr(radian) to 0.0100 Hartrees/Bohr(radian) for both criteria. In all cases, when these convergence criteria were met, the geometries were stable and the total energies changed by less than 0.0003 Hartrees from one iteration to the next. As such, the energies at the transition states could be in error by approximately 2 kcal/mol due to incomplete geometric convergence alone. Considering, however, that the size of our system precludes the verification of the first-order saddle points with frequency calculations performed with *numerical* second derivatives and that the algorithms for frequency calculations with *analytical* second derivatives which are amenable to ECP basis sets[14] are not yet available in commercial quantum chemistry packages, the extra effort required to achieve higher accuracy was neither justified nor feasible. The smooth evolution of the geometries from reactants to products in our initial RHF reaction coordinate calculations provided a less rigorous, yet still valid, indication that the transition state structures were reasonable.[15] In addition, all calculated transition states had a single negative eigenvalue in the final updated Hessian.

A basis set incorporating the ECP2-type effective core potentials of Hay and Wadt[16a] was used for the Rh atom and was chosen over the ECP1-type basis[16b] in deference to other studies[17] which weighed the relative merits of both. With the ECP2-type basis, the outer-core electrons (the $4s^2$ and $4p^6$ for Rh) are treated in the valence space, while for the ECP1 basis, they are treated as part of the pseudopotential. The double-ζ valence functions for Rh[16a] were augmented with an energy-optimized set of 5p functions,[18] yielding a final contraction of (541/541/31). The ECPs of Stevens et al.[19] were used for the remaining non-hydrogen atoms, and a double-ζ contraction was employed for all valence functions except for those of the methyl carbon and hydrogen atoms, which were represented

(9) Peng, C.; Ayala, P. Y.; Schlegel, H. B.; Frisch, M. J. *J. Comput. Chem.* **1996**, *17*, 49−56.
(10) Becke, A. D. *J. Chem. Phys.* **1993**, *98*, 5648−5652.
(11) Lee, C.; Yang, W.; Parr, R. G. *Phys. Rev. B* **1988**, *37*, 785−789.
(12) Frisch, M. J.; Trucks, G. W.; Schlegel, H. B.; Gill, P. M. W.; Johnson, B. G.; Robb, M. A.; Cheeseman, J. R.; Keith, T. A.; Petersson, G. A.; Montgomery, J. A.; Raghavachari, K.; Al-Laham, M. A.; Zakrzewski, V. G.; Ortiz, J. V.; Foresman, J. B.; Cioslowski, J.; Stefanov, B. B.; Nanayakkara, A.; Challacombe, M.; Peng, C. Y.; Ayala, P. Y.; Chen, W.; Wong, M. W.; Andres, J. L.; Replogle, E. S.; Gomperts, R.; Martin, R. L.; Fox, D. J.; Binkley, J. S.; Defrees, D. J.; Baker, J.; Stewart, J. J. P.; Head-Gordon, M.; Gonzalez, C.; Pople, J. A. *Gaussian 94*, Revision D1; Gaussian, Inc.: Pittsburgh, PA, 1995.
(13) Peng, C.; Schlegel, H. B. *Israel J. Chem.* **1993**, *33*, 449−454.
(14) Cui, Q.; Musaev, D.; Svensson, M.; Morokuma, K. *J. Phys. Chem.* **1996**, *100*, 10936−10944.
(15) Ishida, K.; Morokuma, K.; Kormornicki, A. *J. Chem. Phys.* **1977**, *66*, 2153−2156.
(16) (a) Hay, P. J.; Wadt, W. R. *J. Chem. Phys.* **1985**, *82*, 299−310. (b) Hay, P. J.; Wadt, W. R. *J. Chem. Phys.* **1985**, *82*, 270−283.
(17) (a) Sargent, A. L.; Hall, M. B.; Guest, M. F. *J. Am. Chem. Soc.* **1992**, *114*, 517−522. (b) Sargent, A. L.; Hall, M. B. *J. Comput. Chem.* **1991**, *12*, 923−933.
(18) Couty, M.; Hall, M. B. *J. Comput. Chem.* **1996**, *11*, 1359−1370.
(19) Stevens, W. J.; Basch, H.; Krauss, M. *J. Chem. Phys.* **1984**, *81*, 6026−6033.

as single-ζ contractions. The hydrogen atoms of the methyl groups were given a simple STO-3G representation,[20] while those on the thiophene were given a 6-31G representation.[21] As a result of these specifications, which will be referred to as BSI, the total size of the system was 176 basis functions.

Two other basis sets were utilized in this study. A smaller basis set, BSII, which corresponded to a total of 153 functions, was used for the initial RHF partial geometry optimizations in nonredundant internal coordinates and employed a single-ζ contraction for all non-thiophenic carbon atoms and did not include the 5p functions on Rh. Single-point energy calculations involving quadratic configuration interaction with all single and double excitations (QCISD)[22] utilized BSIII, a basis set identical to BSI except that the contraction for the 5d functions was (211), yielding a total of 182 basis functions. In the QCISD calculations, the four lowest occupied and four highest unoccupied orbitals, which contained the 4s and 4p electrons of Rh, were excluded from the active space.

Deformation density calculations and the topological analysis of the charge density[23] were performed through the application of a modified version of MOPLOT.[24] Calculations in which results presented in the atomic orbital basis are transformed to a basis of molecular fragments were carried out with the program GTRAN,[25] which partitions the electron density between interacting fragments through an evaluation of Mulliken gross populations.[26]

Simplifications of the model through substitutions of the Cp* and PMe_3 ligands with Cp and PH_3 groups were *not* employed for two reasons. First, results from preliminary calculations at the RHF level demonstrated that such substitutions resulted in a 40% underestimation of the binding energies for the η^1 and η^2 complexes compared to the results with the larger ligands. Second, experimental studies of benzo[*b*]thiophene binding to $Cp(CO)_2Re$ have demonstrated that the thermodynamic preference for the η^1- and η^2-coordinated complexes *reverses* when the Cp group is replaced by Cp*.[27] That the kinetics of the C−S bond-activation reaction are at least as dependent as the reaction thermodynamics on an accurate description of the electron density at the metal center underscored the need for the full ligands in the computational analysis.

The geometries of the electron-deficient fragments Cp_2W and $Cp^*Re(CO)_2$ were fully optimized, while that for $(PEt_3)_2$-Pt held the P−Pt−P angle fixed at the experimental value of 97.6°. The ethyl groups of both phosphines were replaced with methyl groups.

Results and Discussion

η^1-Coordination of Thiophene. Before we discuss the interaction of thiophene with $Cp^*Rh(PMe_3)$, it is instructive to first examine the molecular orbitals of the constituent fragments. Figure 1 shows the valence molecular orbitals of the thiophene and the rhodium fragments. As noted previously by Harris,[8b] the HOMO of thiophene is not the $2b_1$ orbital predicted by approximate MO calculations but rather is the $1a_2$ orbital which contains the π component of the carbon−carbon double bonds. The LUMO is π antibonding between all adjacent atoms except the distal carbon−carbon bond. For the 16-electron Rh fragment, the 1a′, 1a″, and 2a′ orbitals comprise the t_{2g}-like set of what can be regarded as a pseudo-octahedral coordination complex with two *cis* ligands missing. The 2a″ and 3a′ orbitals make up the e_g-like set. If we set the axis of the molecule such that the 1a′ orbital is designated as the d_{xy} orbital, then the LUMO of this fragment is primarily metal $d_{x^2-y^2}$ in character. Enough metal 5s and 5p mixes in with this

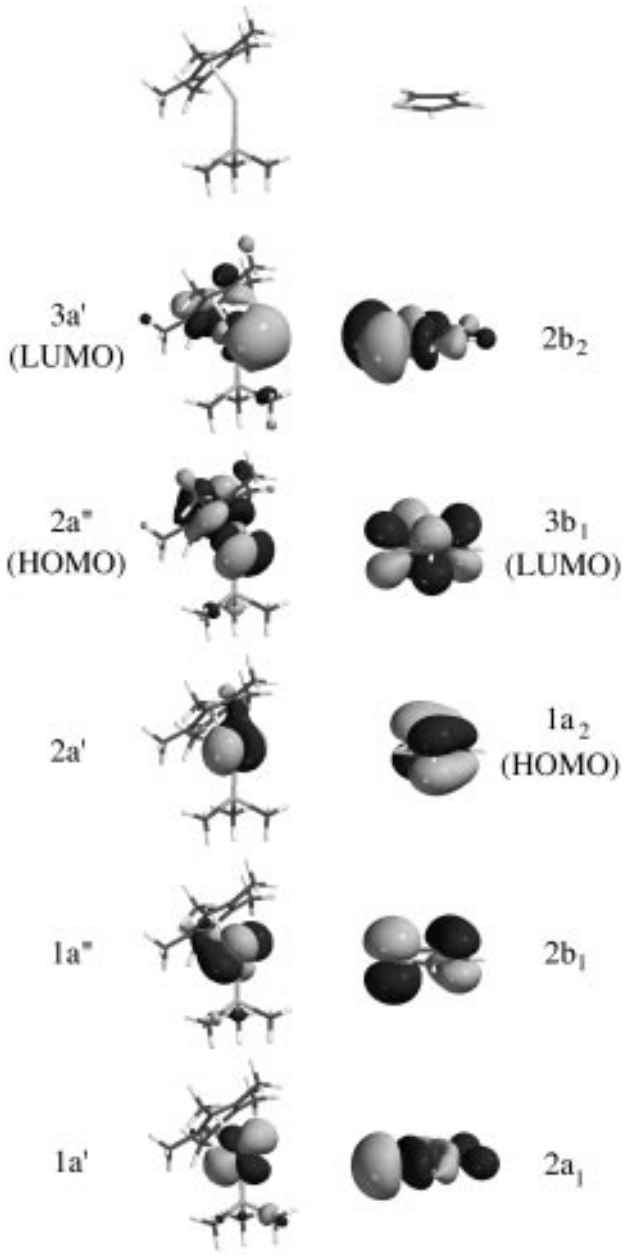

Figure 1. Valence molecular orbitals of thiophene and $Cp^*Rh(PMe_3)$ with symmetry designations in C_{2v} and C_s symmetry, respectively, calculated at the B3LYP/BSI level of theory.

(20) Hehre, W. J.; Stewart, R. F.; Pople. J. A. *J. Chem. Phys.* **1969**, *51*, 2657−2664.
(21) Ditchfield, R.; Hehre, W. J.; Pople, J. A. *J. Chem. Phys.* **1971**, *54*, 724−728.
(22) Pople, J. A.; Head-Gordon, M. *J. Chem. Phys.* **1987**, *10*, 5968−5975.
(23) (a) Bader, R. F. W. *Atoms in Molecules: A Quantum Theory;* Oxford University Press: Oxford, 1990. (b) Bader, R. F. W.; Essen, H. *J. Chem. Phys.* **1984**, *80*, 1943−1960. (c) Bader, R. F. W.; MacDougall, P. J.; Lau, C. D. H. *J. Am. Chem. Soc.* **1984**, *106*, 1594−1605.
(24) Interactive MOPLOT incorporates the programs MOPLOT (Lichtenberger, D.), PLOTDEN (Bader, R. F. W.; Kenworthy, D. J.; Beddal, P. M.; Runtz, G. R.; Anderson, S. G.), SCHUSS (Bader, R. F. W.; Runtz, G. R.; Anderson, S. G.; Biegler-Koenig, F. W.), and EXTREM (Bader, R. F. W.; Biegler-Koenig, F. W.) Sherwood, P.; MacDougall, P. J. 1989.
(25) Sargent, A. L.; Hall, M. B. *GTRAN*; 1990.
(26) Mulliken, R. S. *J. Chem. Phys.* **1955**, *23*, 1833−1840, 1841−1846.
(27) (a) Choi, M.-G.; Robertson, M. J.; Angelici, R. J. *J. Am. Chem. Soc.* **1991**, *113*, 4005-4006. (b) Choi, M.-G.; Angelici, R. J. *Organometallics* **1992**, *11*, 3328−3334.

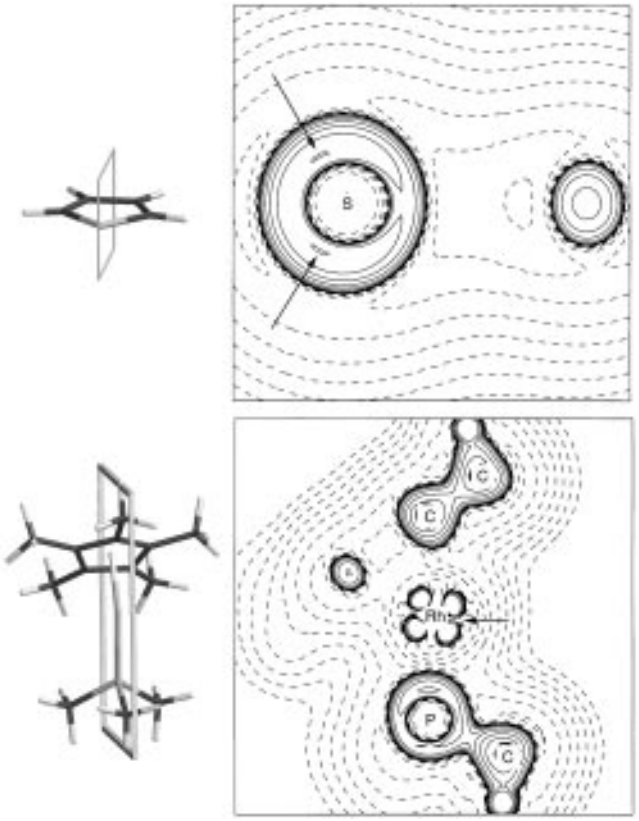

Figure 2. Plots of $-\nabla^2\rho$ for thiophene and Cp*Rh(PMe$_3$) in the specified planes. Regions of local charge concentration ($-\nabla^2\rho > 0$) are denoted by solid contours, while regions of local charge depletion ($-\nabla^2\rho < 0$) are denoted by dashed contours. Ten geometric contours of each sign are plotted. The absolute value of the smallest contour is 0.001953 e/a_o^5.

orbital to generate a dsp hybrid, the large lobe of which extends outward between the two vacant coordination sites.

To understand the formation of the pyramidal η^1-coordinated geometry from an orbital perspective, simple linear combinations of the $2a_1$ and $2b_1$ fragment molecular orbitals (FMOs) of thiophene can be constructed to form the sulfur lone pairs.[6,8e] Thiophene orients itself to maximize the overlap of one of the lone pairs with the LUMO of the Rh fragment while minimizing its steric repulsion with the Cp* and PMe$_3$ groups. This results in the pyramidal sulfur-bound coordination geometry.

An analysis of the topology of the total charge density lends support to this orbital model. Figure 2, which shows plots of the negative of the Laplacian of the total charge density, displays regions of local charge concentration and charge depletion within each of the two interacting fragments. Two regions of local charge concentration are evident around sulfur and correspond to the valence lone pairs. The alignment of one of these lumps of charge concentration with the region of local charge depletion at Rh, shown by the arrow in Figure 2, results in a pyramidal η^1 coordination geometry.

The optimized molecular geometry of **1** is shown in Figure 3, along with the principal orbital interactions of the molecular fragments. Figure 3b shows that 0.26 electron is donated from a sulfur lone pair FMO to the 3a′ LUMO of the metal fragment. The thiophene FMO shown in Figure 3b is one of the linear combinations of

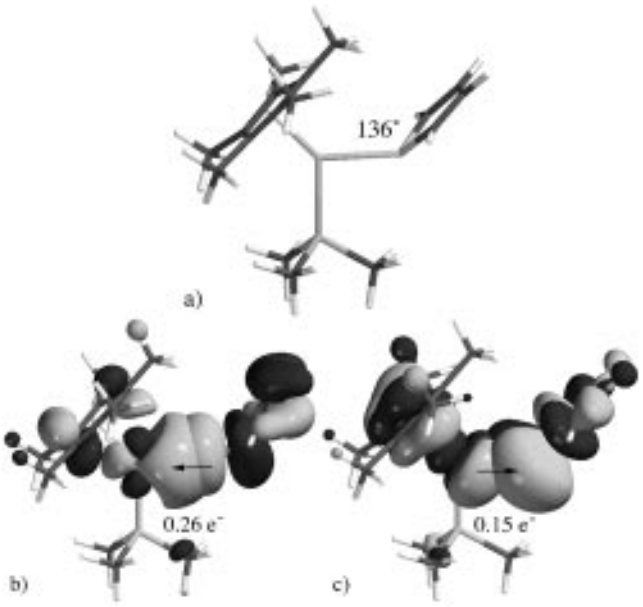

Figure 3. (a) Optimized molecular geometry of the η^1-coordinated intermediate, **1**. (b) FMOs involved in the forward donation of electron density from thiophene to the metal fragment. Orbital character and Mulliken gross populations were determined by transforming the results of the DFT calculations into a basis of molecular orbitals of the interacting fragments. (c) FMOs involved in the back-donation of electron density.

the $2a_1$ and $2b_1$ FMOs. Approximately 0.15 electron is transferred back to the $2b_2$ thiophene FMO from the 2a″ HOMO of the metal fragment. Notice that neither interaction shown in Figure 3b or 3c involves HOMO/LUMO chemistry between fragments; the LUMO of the metal interacts with occupied thiophene orbitals which are two and three levels below the HOMO, while the HOMO of the metal interacts with the thiophene FMO one level above the LUMO. Considering that large energetic separations between molecular fragments result in small interfragment interactions,[28] it is not surprising that the calculated binding energy for **1** is only 16.7 kcal/mol.

The orbital interactions described above between the molecular fragments result in a net transfer of electron density from the thiophene fragment to the metal fragment. To avoid any ambiguity that might be associated with the interpretation of the results from within a particular orbital model, we have analyzed the electron density directly in the form of deformation density plots. Figure 4a shows the deformation density of **1** and corroborates the results of the fragment molecular orbital analysis. The net interaction involves the depletion of density at sulfur in the region of the lone pair and the accumulation of density on the rhodium fragment in the region of the LUMO.

Calculations on the η^1 coordination complex of tetramethylthiophene, **1b**, reveal that 0.31 electron is transferred in the interaction which is analogous to that shown in Figure 3b, while 0.16 electron is involved in the corresponding back-donation. Again, the net transfer is in the forward direction but is larger than that for unsubstituted thiophene, as expected for this ligand.

(28) Hoffmann, R. *Acc. Chem. Res.* **1971**, *4*, 1−9.

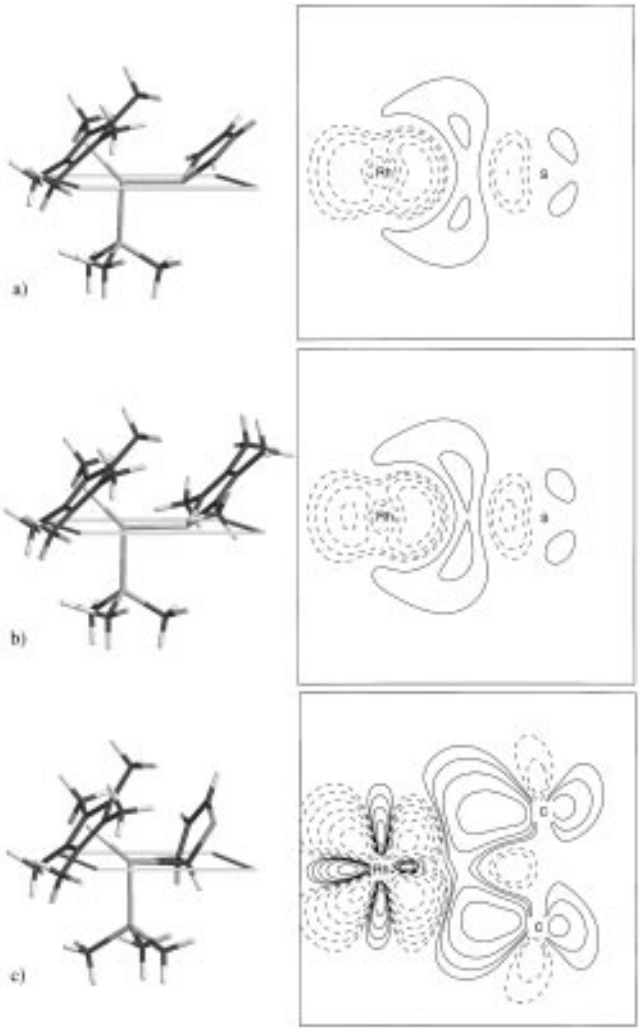

Figure 4. Deformation density plots in the specified planes for (a) the η^1-coordinated thiophene complex (**1**), (b) the η^1-coordinated tetramethylthiophene complex (**1b**), and (c) the η^2-coordinated thiophene complex (**2**). Promolecule densities for the thiophene and metal fragments were subtracted from the total density of the coordination complex. The contours are geometric, with the value of the smallest positive and negative contour equal to ± 0.001953 e/a_o^3. Negative contours are dashed.

The deformation density plot in Figure 4b shows that more density is lost from the sulfur lone pair region and more accumulates in the region of the LUMO on the rhodium fragment. In accord with these results, the calculated binding energy of **1b** is larger at 19.0 kcal/mol. The pyramidal binding angle in **1b** is 132°, compared to 136° in **1**, which indicates that any steric repulsion between the methyl groups on the thiophene and the Cp* is overcome by the stabilizing influence of the stronger Lewis-acid−Lewis-base interaction.

Consistent with the weak binding energy for **1**, the potential-energy surface corresponding to the distortion about the pyramidal binding angle is shallow and exhibits a barrier of only 2.2 kcal/mol, as shown in Figure 5. Two minima appear on this surface: one at $\alpha = 136°$ and the other at $\alpha = 214°$. The former is the global minimum for **1** and corresponds to the distal end of thiophene being positioned closer to the Cp* moiety, while the latter is a local minimum where the distal end of thiophene is closer to the PMe_3 group. The

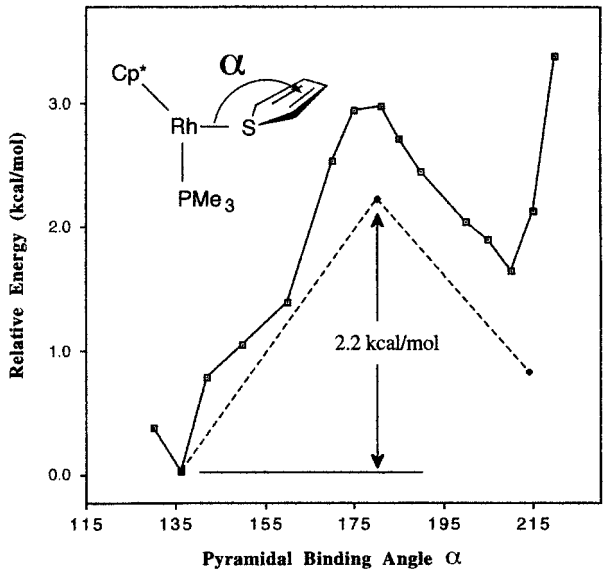

Figure 5. Total energy as a function of the pyramidal binding angle, α, relative to the equilibrium binding angle of the optimized molecular structure of **1**. Energies along the solid line represent single-point calculations for various fixed values of α, whereas energy values along the dashed line involve the reoptimization of all internal coordinates, with the transition state located via the QST2 algorithm.

calculated equilibrium pyramidal binding angle ($\alpha = 136°$) is comparable to the 140° angle found in the isolable η^1-coordinated $Cp^*Re(CO)_2$ complex with thiophene.[29]

C−S Bond-Activation Reaction. The η^1-coordinated complex is an intermediate on the pathway leading to the C−S bond-activation product, and Figure 6 shows the RHF/BSII reaction coordinate corresponding to the ring-opening reaction. On approach to the transition state, the η^1-coordinated thiophene tilts up and rotates in a manner which brings one of the α-carbons in proximity to the Rh atom to facilitate both the formation of the Rh−C bond and the cleavage of the C−S bond. This orientation corresponds to the maximum overlap between the HOMO of the metal fragment and the LUMO of thiophene, which is C−S antibonding in character, allowing for the back-donation of density from the former to the latter and the concomitant scission of the C−S bond. The participation of these two FMOs in the transition state has been noted previously.[7b] Following the cleavage of the C−S bond, the thiophenic moiety flattens back out as the metal continues to insert into the ring. A detailed analysis of the orbital interactions in the ring-opened product has been given elsewhere.[8c]

The structures and relative energetics of **1**, the transition state (**5**), and the C−S bond activation product (**3**) calculated at the DFT/B3LYP/BSI level of theory are shown in Figure 7. As expected, the barrier to the ring-opening reaction decreases with the inclusion of electron correlation. Somewhat unexpected is the large increase in the exothermicity of **3** at the higher level of theory. Other studies have shown that the enthalpy of reaction for a Rh complex undergoing oxidative addition is highly sensitive to the basis set

(29) Angelici, R. J.; Choi, M.-G. *Organometallics* **1991**, *10*, 2436−2442.

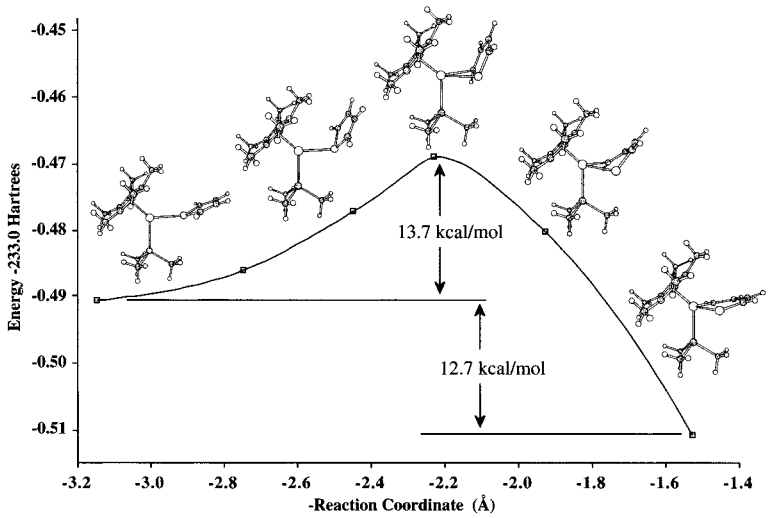

Figure 6. Reaction coordinate for the C−S bond activation of thiophene calculated at the RHF/BSII level of theory. The reaction coordinate variable was defined as the distance from the rhodium atom to the midpoint of the S−C_2 bond. The optimized molecular geometries shown in the diagram correspond to the reaction coordinate variables 3.1476, 2.7476, 2.2285, 1.9285, and 1.5285 Å.

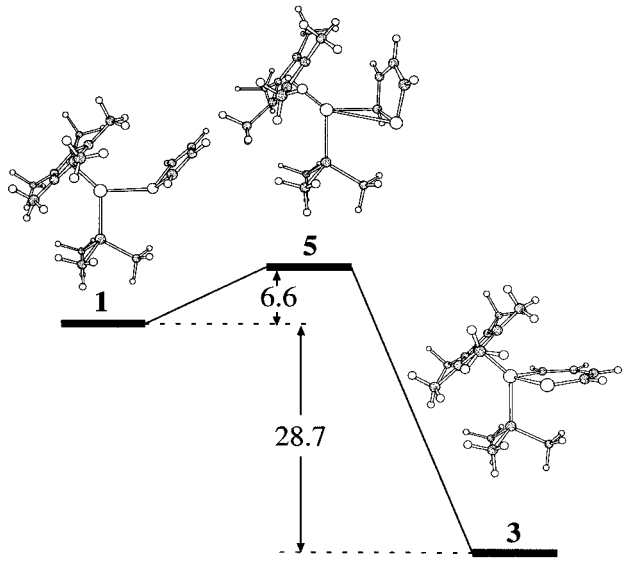

Figure 7. DFT/B3LYP/BSI-optimized geometries and relative energetics for the η^1-coordinated complex (**1**), the transition state for the C−S bond activation reaction (**5**), and the ring-opened product (**3**).

contraction of the 5s orbital,[30] yet BSI utilizes a contraction scheme in accordance with the recommendations made in ref 30, and QCISD/BSIII calculations (vide infra) yield energy splittings comparable to that determined at the DFT/B3LYP/BSI level of theory.

Relevant geometric parameters for the optimized molecular geometries shown in Figure 7 are listed in Table 1. It is interesting to note that in **5** the Rh−S distance is 29% longer than the sum of the covalent radii, while the Rh−C_2 and the S−C_2 distances are within 8% and 5%, respectively, of the sum of the covalent radii. Although the C−S bond scission and Rh−C bond-formation steps involved in the transformation of **1** to **3** are concerted to some extent, the geometry of **5** suggests that the progress of the bond-formation step is more advanced at the transition state than is the bond-scission step.

Included in Table 1 are the calculated and experimental[31] geometric parameters for the C−S bond-activation product of 2,5-dimethylthiophene, **3a**. As noted in other studies which have utilized DFT/B3LYP methods,[32] the agreement between theoretical and experiment structures is good. The largest deviation is in the Rh−P bond, where the difference between theory and experiment is 0.141 Å. All remaining bond distances are in agreement to less than 0.1 Å, and the bond angles differ by 2° or less. Regarding the planarity of the metallathiabenzene ring for the calculated structure of **3a**, the Rh atom lies 0.8 Å above the plane defined by atoms C_2, C_4, and S while the corresponding value from the experimental structure is 0.7 Å. Without the methyl groups on thiophene, the distortion from planarity is greatly reduced. In **3**, the distortion is only 0.2 Å, while for the tetrasubstituted complex, **3b**, it is 1.0 Å. The effect of increased methyl substitution on the planarity of the metallathiabenzene ring is easily seen in Figure 8.

Unlike thiophene and 2,5-dimethylthiophene, the C−S bond-activation reaction of tetramethylthiophene has not been experimentally observed and the optimized structure of **3b** shown in Figure 8 appears to support the suggestion that the buttressing effect of forcing the four methyl groups on the six-membered ring into coplanarity is a possible cause for the lack of reactivity.[5] The calculated energetics corroborate this conclusion as well; while the binding energies for the η^1 complexes of thiophene, 2,5-dimethylthiophene, and tetramethylthiophene increase in a fairly uniform fashion (16.7, 18.2, and 19.0 kcal/mol, respectively), the enthalpies for metal insertion into the η^1 complex decrease less uniformly (−28.7, −23.0, and −11.8 kcal/mol). Note the precipitous decrease which accompanies the reaction involving tetramethylthiophene.

Despite this abrupt decrease, the calculated enthalpy

(30) Couty, M.; Bayse, C. A.; Jiménez-Cataño, R.; Hall, M. B. *J. Phys. Chem.* **1996**, *100*, 13976−13978.

(31) Jones, W. D.; Dong, L. *J. Am. Chem. Soc.* **1991**, *113*, 559−564.

(32) Cui, Q.; Musaev, D. G.; Morokuma, K. *Organometallics* **1997**, *16*, 1355−1364.

Table 1. Selected Geometric Parameters for the DFT/B3LYP/BSI-Optimized Structures[a]

geometric param	reactants	1	1b	5	3	3a	3a (expt.[b])	3b	2	7	6	4	8	4a	9
Rh−P	2.335	2.354	2.351	2.369	2.366	2.384	2.243	2.395	2.377	2.367	2.348	2.352	2.369	2.360	2.373
Rh−S		2.414	2.415	3.206	2.429	2.430	2.336	2.411	3.482	3.485	3.247	3.402	3.394	3.376	3.440
Rh−C_2		3.688	3.659	2.196	2.032	2.055	2.067	2.056	2.124	2.113	2.202	2.036	2.063	2.029	2.114
Rh−C_3		4.678	4.615	2.716	3.122	3.083		3.104	2.186	3.206	2.803	3.132	3.203	3.150	3.216
S−C_2	1.813	1.832	1.855	1.884	3.271	3.228		3.143	1.887	1.867	1.884	1.854	1.863	1.871	1.865
C_2−C_3	1.392	1.386	1.387	1.437	1.381	1.382	1.35	1.387	1.477	1.415	1.435	1.406	1.408	1.401	1.412
C_3−C_4	1.461	1.468	1.490	1.443	1.478	1.478	1.44	1.507	1.482	1.454	1.442	1.465	1.462	1.465	1.455
C_4−C_5	1.392	1.386	1.387	1.399	1.381	1.380	1.34	1.384	1.380	1.392	1.403	1.391	1.389	1.390	1.392
S−C_5	1.813	1.832	1.855	1.803	1.815	1.836	1.741	1.843	1.836	1.810	1.794	1.819	1.814	1.821	1.813
Rh−H		3.951		2.774	2.652				2.789	1.671	2.745	1.561	1.549	1.563	1.680
C_2−H	1.087	1.087		1.092	1.104				1.094	1.350	1.091	2.441	2.336	2.388	1.339
Rh−X[c]	1.977	2.003	2.006	2.138	2.006	2.006		2.008	2.031	2.031	2.101	2.005	2.035	2.003	2.025
P−Rh−X	141.9	134.3	134.1	128.9	133.4	132.1		131.5	128.6	130.4	130.8	134.9	130.8	134.9	131.3
S−Rh−C_2		25.5	26.8	34.9	93.9	91.7	92.5	89.1			34.1				
S−Rh−P		92.3	91.6	84.0	88.7	86.5	86.5	85.2			97.9				
Rh−S−C_4		120.0	117.4	96.2	109.2	107.8	109.7	105.1			97.4				
Rh−C_2−C_3		128.5	126.2	94.5	131.4	126.4	124.0	127.6	72.2	129.5	98.6	130.1	133.8	132.4	130.6
C_2−C_3−C_4	113.3	113.6	114.3	115.7	129.1	130.7	131.5	127.2	112.1	116.1	114.9	115.9	116.8	116.1	116.2
C_3−C_4−C_5	113.3	113.6	114.3	113.9	127.5	128.0	128.3	125.1	115.1	113.8	113.6	113.7	113.7	114.0	113.9
C_2−Rh−H				21.6					20.6	39.7	22.2	84.3	79.2	82.2	39.3
P−Rh−C_2−S				278.3				274.8	198.5	197.2	250.9	253.9	154.0	68.7	40.0

[a] Atoms are numbered sequentially around the thiophene ring, beginning with sulfur. [b] Reference 31. [c] X represents the centroid of the Cp* ring.

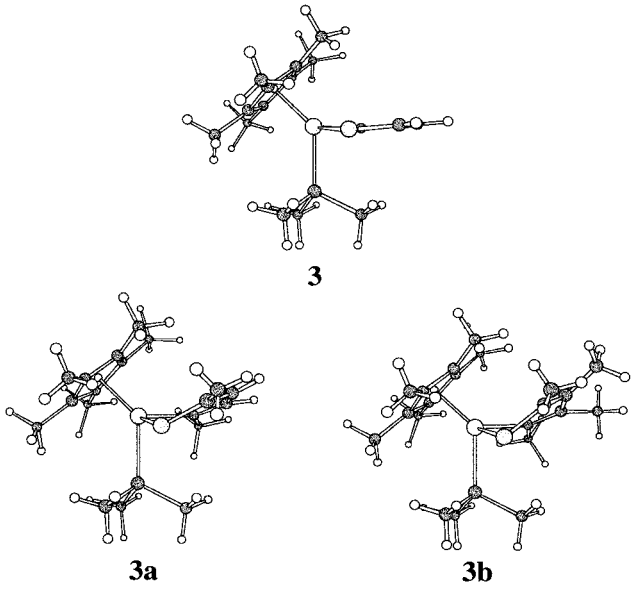

Figure 8. Optimized molecular geometries of the ring-opened complexes of thiophene (**3**), 2,5-dimethylthiophene (**3a**), and tetramethylthiophene (**3b**), viewed from a perspective which highlights the planarity (or lack thereof) of the metallathiabenzene ring.

for metal insertion into tetramethylthiophene is negative and appears to predict a spontaneous reaction from a thermodynamic standpoint. However, it is important to remember that temperature effects have not been accounted for in our calculation of ΔH. Qualitatively, the entropy contribution to the reaction which combines the free fragments will be negative and will decrease the exothermicity. Whether or not this contribution, along with corrections for zero-point energies and solvent effects, is large enough to yield a positive ΔG remains to be determined. Unfavorable kinetics, however, would prevent the reaction from occurring under reasonable conditions despite favorable thermodynamics. The fact that the C−S bond-activation reaction of 2,5-dimethylthiophene has been observed experimentally[5] has served as the cornerstone for the argument that sterics do not prevent the C−S activation reaction of tetramethylthiophene. Considering, however, that the calculated geometry of **5** involves the close proximity of the *distal* carbons (carbons 3 and 4) on thiophene with the Cp* group of the metal fragment suggests that substitution at carbons 3 and 4 may contribute to the steric component of the barrier more than substitution at the 2 and 5 positions. Of the geometric parameters listed in Table 1, the Rh−X distance (i.e., the distance between Rh and the centroid of the Cp*) is the largest for complex **5**, while the P−Rh−X angle is nearly the smallest. Taken together, these values reflect the steric interference caused by the close approach of the back end of thiophene with the Cp* group in **5**. While experimental studies have demonstrated the insertion reaction with just a single methyl group on one of the distal carbons (with a significant preference for one of the two insertion products),[5] the disubstituted 3,4-dimethylthiophene may be as unwilling to insert the metal as tetramethylthiophene, based on these arguments.

η^2 Coordination of Thiophene. Figure 9a shows the optimized molecular geometry of the η^2-coordinated intermediate, **2**, postulated for the reaction of thiophene with Cp*RhPMe$_3$. The two principal orbital interactions between the molecular fragments in **2** consist of the forward donation of density from the $1a_2$ FMO of thiophene to the 3a′ FMO of the metal fragment, as shown in Figure 9b, and the back-donation of density from the 2a″ FMO of the metal to the $3b_1$ FMO of thiophene, as shown in Figure 9c. Notice that, unlike the interactions of **1**, these interactions describe HOMO/LUMO chemistry; the HOMO of thiophene donates to the LUMO of the metal and the HOMO of the metal back-donates to the LUMO of thiophene. One consequence of the small energetic separation between the HOMO/LUMO interactions of the molecular fragments is strong interfragment interactions,[28] and the calculated binding energy of **2**, 32.2 kcal/mol (compared to 16.7 kcal/mol for **1**), is testimony to this effect.

The large magnitude of electron density transferred

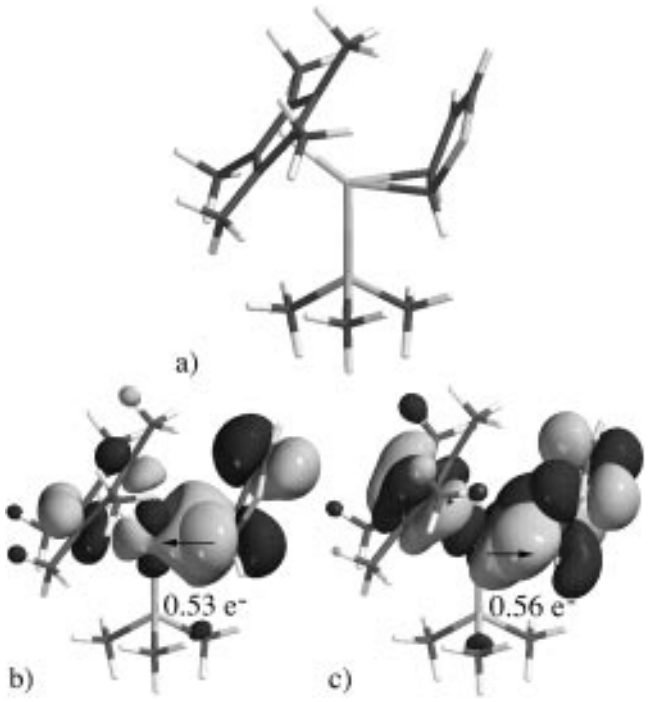

Figure 9. (a) Optimized molecular geometry of the η^2-coordinated intermediate, **2**. (b) FMOs involved in the forward donation of electron density from thiophene to the metal fragment. (c) FMOs involved in the back-donation of electron density.

between the molecular fragments also testifies to the strength of the interaction. Notice that the fragment analysis suggests that the back-donation is more pronounced than the forward donation, yielding a net transfer of density from the metal to thiophene. The deformation density plot shown in Figure 4c supports this conclusion. Notice, too, that the near cancellation of the forward and reverse donation of density is evident in Figure 4c along the axis connecting the Rh atom to the centroid of the carbon−carbon bond. The accumulation of density appears primarily to the sides of this axis in the region where the overlap of the four FMOs is minimal.

Further evidence for the magnitude of the back-donation in **2** is found in the bond distances of thiophene listed in Table 1. Notice that the S−C bond distance is essentially the same length as it is in **5** and that all other distances around the ring, except the noncoordinating C−C double bond, are longer than those in **5**. Although the P−Rh−X angle in **2** is small to minimize the repulsion between thiophene and the Cp* group, the Rh−X distance is shorter than it is in **5**, indicating that the strength of the Rh−Cp* interaction is not sacrificed in **2**.

Direct η^2 to η^1 Interconversion. Jones and coworkers proposed that the intramolecular rearrangement of C−H bond-activation products to the C−S activation product involved the direct interconversion of intermediates **2** and **1**,[5] as shown by the dashed line in Scheme 1. Additional support for this rearrangement pathway has come from a subsequent study which demonstrated the interconversion of the η^2 and η^1 complexes of benzo[*b*]thiophene with Cp*(CO)$_2$Re and for which no C−S or C−H bond activation products were observed.[27] The structure of **6**, which is the calculated

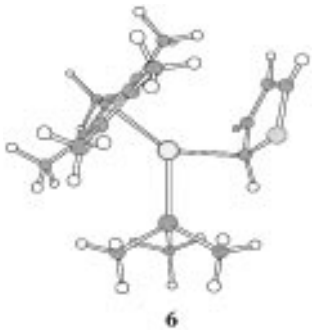

Figure 10. Optimized molecular geometry of the transition state **6** which connects intermediates **2** and **1**.

transition state for the conversion of **2** to **1**, is shown in Figure 10. While **6** may appear to be very similar to **5**, the principal distinction between the two is in the P−Rh−C$_2$−S dihedral angle, which differs by nearly 30°. This dihedral angle essentially defines how close the sulfur atom is to the plane illustrated in Figure 4. In **5** the sulfur of thiophene is essentially in this plane, while in **6** it is still far above the plane. As illustrated in Figure 4c, the sulfur atom lies above the plane in **2**. As **2** evolves to **1**, the thiophenic ring rotates and the sulfur atom moves downward toward the plane. Recalling from Figure 2 that above and below this plane reside regions of charge concentration on the metal atom, significant repulsions will result between these concentrations of charge on rhodium and those on sulfur as the sulfur atom approaches the rhodium atom from above the plane. This repulsion, therefore, contributes to the barrier for the interconversion of **2** to **1**.

Reactions Involving C−H Bond Activation. Although two C−H bond activation products are possible for thiophene,[5] our computational studies focused exclusively on the 2-thienyl metal hydride product, **4**, and the results are shown in Figure 11. The mechanism of the activation reaction which carries intermediate **2** to product **4** is similar to that reported for the oxidative addition of ethylene to CpIrPH$_3$[33] and will, therefore, not be discussed in detail. Of particular importance to the C−H bond-activation reaction is the back-donation of density from the 2a″ HOMO of the metal fragment to the 3a$_1$ thiophene FMO (the fourth lowest unoccupied FMO, not shown in Figure 1) which is C−H σ antibonding in character.

Two rotamers of the 2-thienyl metal hydride product are possible. The oxidative addition of thiophene which begins with intermediate **2** yields one of the isomers, product **4**. Rotation about the Rh−C$_2$ bond in **4** yields rotamer **4a**, and the barrier connecting the two is small. Both rotamers were observed experimentally: the crystal structure of the related 2-thienyl metal chloride was disordered at sulfur over the two possible rotamers, and the refined populations indicated little preference for either orientation,[5] in agreement with a small barrier. The significance of this facile isomerization is twofold. First, our computational analysis indicates that rotamer **4a** is the thermodynamically favored product; the energy of **4** is 0.5 kcal/mol *above* that of **2**, while **4a** is 0.1 kcal/mol *below* **2**. The relative energies of **4** and **4a**

(33) Silvestre, J.; Calhorda, M. J.; Hoffmann, R.; Stoutland, P. O.; Bergman, R. G. *Organometallics* **1986**, *5*, 1841−1851.

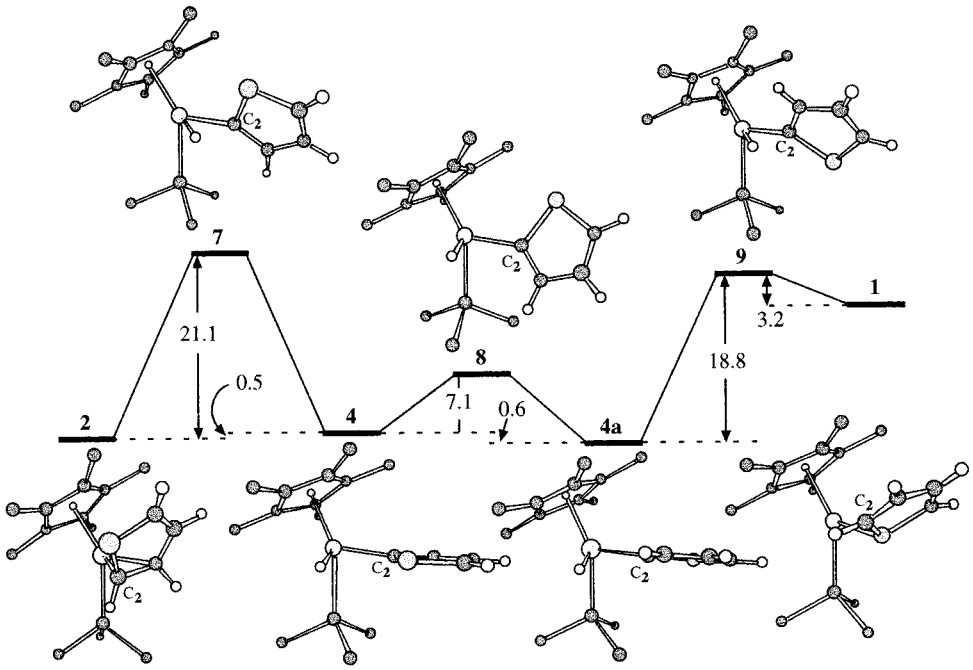

Figure 11. Schematic illustrating the optimized molecular geometries and relative energetics of the C−H bond activation of **2** and the subsequent rotational isomerization and reductive elimination of the product. For clarity, the methyl hydrogens are not shown and the C_2 atom of thiophene is labeled.

calculated at the QCISD/BSIII level of theory concur with the DFT/B3LYP/BSI energies (vide infra).

The second and perhaps more interesting point of significance regarding the rotational isomerization is that the reactivity of rotamer **4a** provides a new intramolecular pathway for the rearrangement of C−H-activated products to the C−S-activated product. The essence of the new pathway is that the reductive elimination of thiophene from rotamer **4a** yields the η^1-coordinated intermediate, **1**, while the reductive elimination of thiophene from **4** simply yields **2**, as this reaction is the microscopic reverse of the oxidative-addition reaction which began with **2**. The reductive elimination from **4** involves the migration of the C_2 atom of the thienyl group (i.e., the carbon bonded to the Rh) toward the hydride to begin to reform the C−H bond. This movement brings the C_2−C_3 double bond of the thienyl group in proximity to Rh and allows the η^2-coordinated interaction to be reestablished. In contrast, as C_2 migrates toward the hydride in the reductive-elimination reaction which begins with **4a**, the sulfur atom is drawn close to Rh allowing the η^1-coordinated interaction to form.

The calculated barrier for this new rearrangement pathway is 18.8 kcal/mol, which is lower than that calculated for the direct interconversion of **2** to **1**. Although higher levels of theory (more extensive inclusion of electron correlation, larger basis sets, and thermochemical corrections) are required before much certainty can be associated with the relative barrier heights, these results suggest the possibility of a new intramolecular rearrangement pathway connecting the C−H bond-activated products with the C−S bond-activation product, as shown in Scheme 2. Viewed in reverse, it also suggests the possibility of a new low-energy C−H bond activation pathway and, most notably, one which does *not* proceed through the η^2-coordinated intermediate.

The movement of thiophene from its position in **1** to that in **9** involves the lateral movement of the sulfur atom along the plane depicted in Figure 4a until the C−H bond is in proximity to the HOMO of the metal fragment. This orientation facilitates the transfer of electron density into the C−H antibonding orbital. The energetic cost of this movement is low since it avoids pointing the lone pair charge concentrations on sulfur at the charge concentrations which exist above and below the rhodium (illustrated in Figure 2). Coupled to the relative instability of **1**, the overall result is a low-energy barrier to C−H activation.

The overall calculated reaction profile is shown in Scheme 2. No attempt was made to calculate the barriers on the pathways connecting the free fragments to **1** and **2**. The experimental work of Jones and coworkers[5] determined that the barrier leading to **2** was higher than that leading to **1**. This result is understandable in light of the optimized structures of **1** and **2**. In the former, the geometric parameters differ little compared to those of the free fragments. In the latter, however, the deviations are large, particularly within the thiophene fragment. Not only are most bond distances significantly elongated, but two of the hydrogen atoms are bent significantly away from the thiophenic plane (dihedral C_5−C_4−C_3−H = 146.5°, dihedral C_5−S−C_2−H = 143.3°). Recalling that under the low-temperature experimental conditions products **3** and **4** are formed in parallel.[5] With the larger barrier corresponding to the η^2 addition of thiophene, addition occurs preferentially in the η^1-coordinated mode to yield **1**, which subsequently undergoes C−S or C−H bond activation to yield the observed products. Little of **2** is formed under these conditions. If this were not the case, one would expect to be able to detect the presence of **2** under low-temperature conditions due to its relative thermodynamic stability. Once the reaction mixture is heated to room temperature, intramolecular rearrange-

Scheme 2

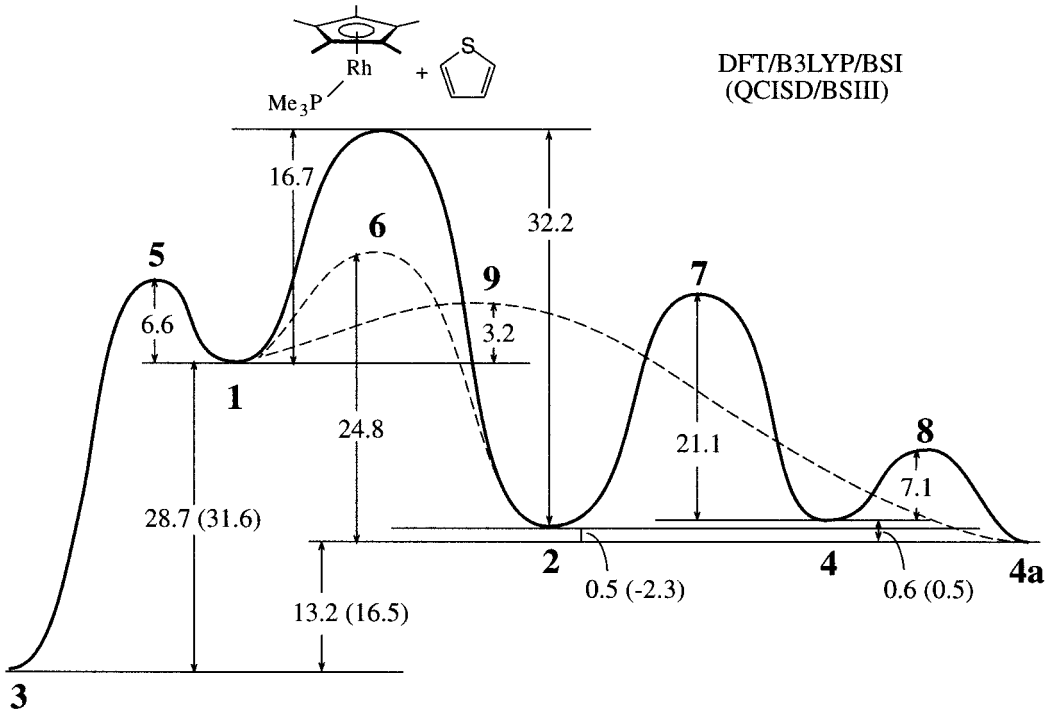

ment occurs via pathways involving **9** or **6** and leads to the complete conversion of product to the thermodynamic sink, **3**.

Energies calculated at the QCISD/BSIII level are shown in parenthesis in Scheme 2. The agreement with DFT/B3LYP/BSI energies is good. Qualitatively, nothing changes except that the QCISD energy for **2** is 2.3 kcal/mol *lower* than that for **4a**, a result which is known to be in disagreement with experiment. As mentioned previously, the energies reported in this paper do not account for zero-point or thermochemical corrections for the reasons mentioned in the Theoretical Details section. While the corrections are a necessary prerequisite to a meaningful comparison of theoretical (Scheme 2) and experimental (Scheme 1) energies, the qualitative agreement between the two levels of theory provides an important measure of veracity. And although the two levels of theory disagree over the relative energetic ordering of **4** and **2**, the magnitude of the splittings is quite small and could easily be overridden by the inclusion of the thermochemical corrections.

Reactivity of Other Metal Fragments. Other electron-deficient metal fragments have been investigated regarding their reactivity toward the C−S bond activation of thiophene. Among them are (triphos)RhH[34] (**10**), (PMe_3)$_3$IrCl[35] (**11**), Cp_2W[36] (**12**), Cp*Re(CO)$_2$[27] (**13**), and (PEt_3)$_2$Pt[37] (**14**). The similarities between **10**, **11**, and Cp*Rh(PMe_3) are several; each one is a 16-electron fragment which contains a d^8 metal and has a four-coordinate ligand field that can be viewed as a pseudo-octahedron with two *cis* ligands missing. One would expect the fragment molecular orbitals to resemble those shown in Figure 1 and that the C−S bond activity would be similar. This is, indeed, the case. Metal fragments **12**, **13**, and **14**, however, contain d^4, d^6, and d^{10} metals, respectively, are 16-electron (**12**, **13**) or 14-electron (**14**) fragments, and have distinctly different ligand fields. Despite these differences, however, the counterparts to the 3a′ and 2a″ orbitals of the Cp*Rh(PMe_3) fragment (Figure 1) are evident in the valence molecular orbitals of fragments **12**, **13**, and **14** and are shown in Figure 12. As mentioned in the preceding discussion, it is crucial for these FMOs to be the HOMO and LUMO of the metal fragment if they are to exhibit similar reactivity toward thiophene. In **12**, the energetic ordering of the 2a′ and 2a″ FMOs is reversed from that in Figure 1, which means that the 2a″ FMO shown in Figure 12 is actually the SHOMO for **12**. However, the HOMO/SHOMO splitting between these orbitals is only 0.00268 Hartrees (1.68 kcal/mol), which suggests that the 2a″ FMO is essentially as energetically accessible to the LUMO of thiophene as the 2a′ FMO, which is higher in energy.

Among these varied metal fragments, only fragment **13** fails to undergo metal insertion into thiophene. Other fragments, including $CpFe(CO)_2^+$,[38a] Cp(CO)(PPh_3)Ru^+,[38b] $Cp(CO)_2Ru^+$,[38c] and Cp*$IrCl_2$,[38d] all contain d^6 metals, have similar supporting ligation, and fail to undergo the metal-insertion reaction. While the reason for this lack of reactivity could be generally categorized as thermodynamic or kinetic, our preliminary analysis suggests that it is a combination of both.

(34) (a) Barbaro, P.; Bianchini, C.; Meli, A.; Peruzzini, M.; Vacca, A.; Vizza, F. *Organometallics* **1991**, *10*, 2227−2238. (b) Bianchini, C.; Jiménez, M. V.; Meli, A.; Vizza, F. *Organometallics* **1995**, *14*, 3196−3202.

(35) Selnau, H. E.; Merola, J. S. *Organometallics* **1993**, *12*, 1283−1591.

(36) Jones, W. D.; Chin, R. M.; Crane, T. W.; Baruch, D. M. *Organometallics* **1994**, *13*, 4448−4452.

(37) (a) Garcia, J. J.; Maitlis, P. M. *J. Am. Chem. Soc.* **1993**, *115*, 12200−12201. (b) Garcia, J. J.; Mann, B. E.; Adams, H.; Bailey, N. A.; Maitlis, P. M. *J. Am. Chem. Soc.* **1995**, *117*, 2179−2186.

(38) (a) Goodrich, J. D.; Nickias, P. N.; Selegue, J. P. *Inorg. Chem.* **1987**, *26*, 3424−3426. (b) Benson, J. W.; Angelici, R. J. *Organometallics* **1992**, *11*, 922−927. (c) Benson, J. W.; Angelici, R. J. *Organometallics* **1993**, *12*, 680−687. (d) Rao, K. M.; Day, C. L.; Jacobson, R. A.; Angelici, R. J. *Inorg. Chem.* **1991**, *30*, 5046−5049.

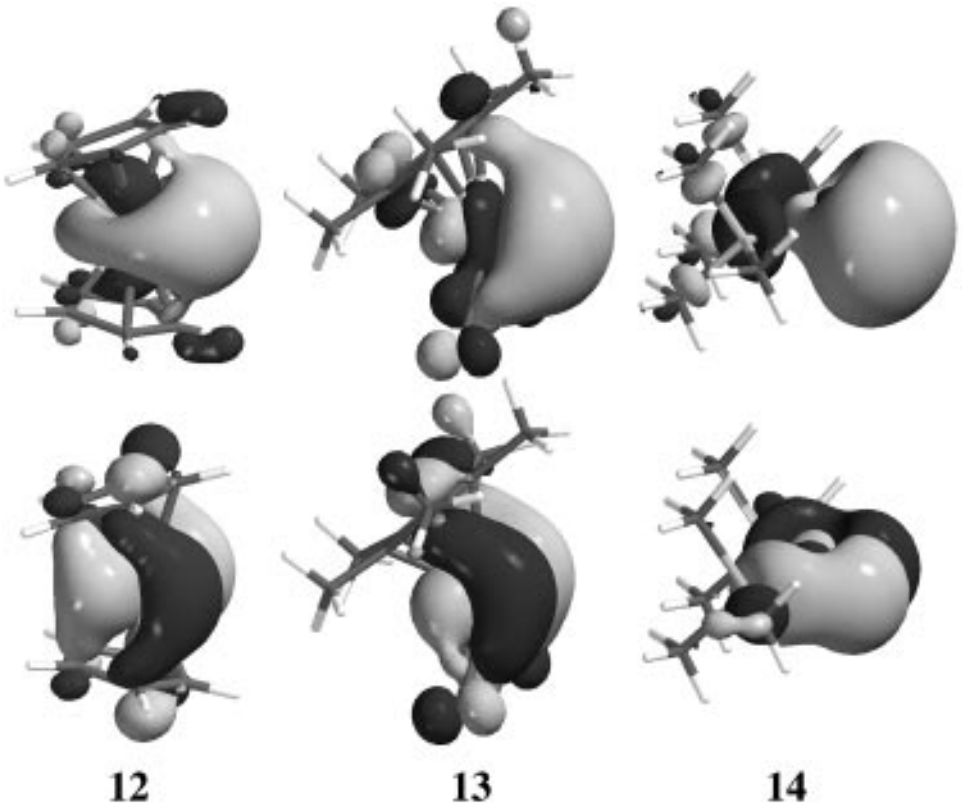

Figure 12. Frontier molecular orbitals of the optimized electron-deficient fragments Cp_2W (**12**), $Cp^*Re(CO)_2$ (**13**), and $Pt(PMe_3)_2$ (**14**).

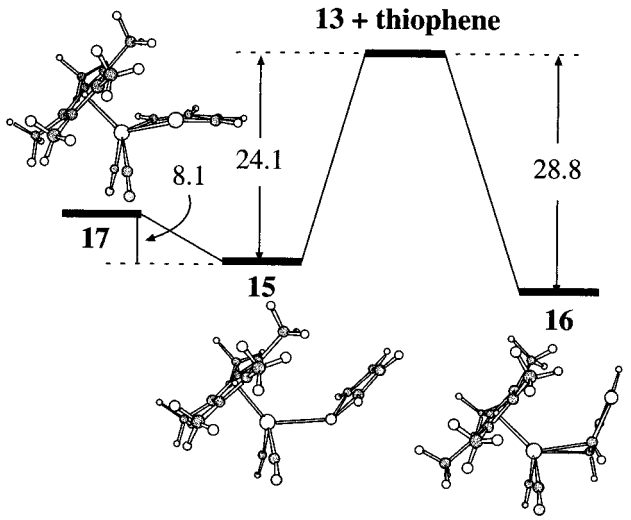

Figure 13. Optimized geometries and relative energetics of the η^1 (**15**), η^2 (**16**), and ring-opened (**17**) complexes of $Cp^*Re(CO)_2$ and thiophene.

The calculated structures and relative energetics for the η^1 (**15**), η^2 (**16**), and ring-opened (**17**) complexes of thiophene with **13** are shown in Figure 13. Two features of the energy diagram are readily apparent. First, the relative instability of **17** and the unusual puckering of the metallathiabenzene ring argue in favor of unfavorable thermodynamics. For the seven-coordinate complex to adopt the geometry of a four-legged piano stool, the metallathiabenzene ring puckers in the direction of the Cp* ligand, a feature not observed in other ring-opened complexes. The Re−S, Re−C_2, and Re−X (X = centroid of Cp*) distances are 2.572, 2.175, and 2.062 Å, respectively, the former two of which are 0.143 Å longer than the analogous distances in **3**. Considering that the Re−S distance in **15** is only 0.100 Å longer than the analogous distance in **1**, the long Re−S and Re−C distances in **17** reflect more than just a change of metal atom, they reflect a weak bonding interaction.

In accord with the analysis of Palmer, Carter, and Harris, which examined the electronic structure of ring-opened complexes,[8c] the long Re−S and Re−C distances translate into a weak orbital interaction between the HOMO of the metal fragment and the LUMO of the ring-opened thiophene fragment. For the ring-opened thiophene fragment, the LUMO is C−S σ antibonding in character. The root of this weak interaction is a large energy difference between the interacting FMOs; the participation of the carbonyl π^* orbitals in the HOMO of the metal fragment significantly lowers the energy of this orbital and increases its energetic separation with the LUMO of the thiophene fragment.

The second noteworthy feature of Figure 13 is the comparable stabilities of **15** and **16**. The difference in binding energies between them is only 4.7 kcal/mol, whereas it was 15.5 kcal/mol between **2** and **1**. Compared to **2**, the binding energy in **16** has decreased by 3.4 kcal/mol, and an analysis of the interacting fragments reveals that this is a result of the decreased back-donation of density which occurs between the 2a″ FMO of **13** and the $3b_1$ FMO of thiophene. Only 0.44 electron is transferred in this interaction, compared to 0.56 electron for the corresponding interaction in **2** (Figure 9). Participation of the carbonyl π^* orbitals in the 2a″ FMO of **13**, which can be seen in Figure 13, results in the delocalization of electron density from the metal onto the carbonyl ligands and a consequent reduction

in the basicity of the fragment. The participation of the carbonyl π^* orbitals also affects the forward donation of density in **16**; 0.61 electron is donated from the $1a_2$ FMO of thiophene to the 3a′ FMO of **13**, compared to only 0.53 electron in the corresponding interaction of **2**. The effect of the carbonyl groups is one which reduces the metal-to-ligand back-donation of density but enhances the density flow in the reverse direction. Unlike **2**, the net transfer of density in **16** is from the ligand to the metal. That the binding energy of **16** is still large indicates that the enhanced forward donation mitigates the restricted back-donation to a large degree and underscores the fact that the η^2 binding mode relies heavily on the transfer of density in both directions. Without the ability to backdonate electron density from the 2a″ FMO, however, **13** is ineffective as a catalyst of C−S and C−H activation reactions.

A fragment analysis of **15** reveals that 0.37 electron is transferred from the thiophene lone pair to the LUMO of the metal fragment, while only 0.1 electron is involved in back-donation. Compared to the analogous interactions in **1** where the donation of density in the two directions was of more equal magnitude and the binding energy was smaller, the large binding energy of **15** is testimony to the fact that the S-bound η^1 coordination mode primarily utilizes the electron-donor ability of thiophene. Additional calculations which examine the extent to which steric and electronic factors separately contribute to the relative stabilites of complexes **15**−**17** are in progress and will be reported in another paper.[39]

Conclusions

In summary, of the two intermediates on the pathways leading to the C−S and C−H bond activation of thiophene with Cp*Rh(PMe$_3$), the η^2-coordinated intermediate, **2**, exhibits tighter binding and greater thermodynamic stability as a result of the smaller energy differences between the molecular orbitals of the interacting fragments. The DFT/B3LYP binding energy of **2** is 32.2 kcal/mol. Less stable is the η^1-coordinated intermediate, **1**, for which the calculated binding energy is 16.7 kcal/mol. The transition state which connects **1** to the C−S bond-activation product, **3**, has a calculated barrier of 6.6 kcal/mol and exhibits a structure in which the distal carbons of thiophene are in close proximity to the Cp* group. In this orientation, the overlap between the LUMO of thiophene and the HOMO of the metal fragment is maximized to facilitate the cleavage of the C−S bond and the formation of the Rh−S and Rh−C bonds. The structure of **3** suggests that the formation of the Rh−C bond precedes both the cleavage of the S−C bond and the formation of the Rh−S bond.

The C−H bond-activation reaction of **2** is accompanied by a substantial barrier of 21.1 kcal/mol and is slightly endothermic (0.5 kcal/mol). A small rotational barrier (7.1 kcal/mol) connects the product **4** with its rotamer **4a**, which is 0.1 kcal/mol exothermic with respect to **2**. The reductive elimination of thiophene from **4a** yields **1** directly, which can then proceed to the C−S bond-activated product. The reductive-elimination reaction, which has a barrier of 18.8 kcal/mol, provides a new low-energy route to the intramolecular rearrangement of **4** to **3**. Viewed in reverse, this suggests that access to the C−H bond-activation products is not restricted to the pathway involving the η^2-coordinated intermediate, **2**, but that the C−S- *and* C−H-activated products are both accessible through the η^1-coordinated intermediate, **1**. Considering that a larger barrier exists for the formation of **2** compared to **1** and that another large barrier separates the C−H activation product **4** with **2**, one would not expect to observe **2** under low-temperature conditions despite its large thermodynamic stability. QCISD energy calculations, which were performed on all equilibrium structures of the coordinated complexes, corroborated the relative energetics determined at the DFT/B3LYP level of theory with a single exception. This exception involved the stability of **2**, which was calculated to be 2.3 kcal/mol more stable than **4a**. Little emphasis was placed on this discrepancy in light of the fact that the magnitude of the difference in splitting was small and that thermochemical corrections, which could not feasibly be performed for this system, would likely reverse this ordering.

A common characteristic of the coordinatively unsaturated metal fragments which undergo C−S and C−H bond-activation reactions is a metal-based HOMO/LUMO pair of FMOs which protrude into the vacant coordination site and which are antisymmetric and symmetric, respectively, in the plane of addition. While the Cp*Re(CO)$_2$ fragment, **13**, possesses this characteristic, it is unreactive toward thiophene activation. Our preliminary studies have revealed that the ring-opened product, **17**, is endothermic with respect to the η^1-coordinated complex, **15**, by 8.1 kcal/mol and that this instability, along with the lack of reactivity toward C−S and C−H bond activation, is due to the presence of the electron-withdrawing carbonyl ligands.

Acknowledgment. We thank the donors of the Petroleum Research Fund, administered by the American Chemical Society (Grant No. 29526-GB6), for partial support of this research. We also thank the North Carolina Supercomputer Center for their continued support of this research.

Supporting Information Available: Tables of the Cartesian coordinates of the optimized molecular geometries for complexes **1**−**17** (except **10** and **11**) (20 pages). Ordering information is given on any current masthead page.

OM970585E

(39) Sargent, A. L.; Cheek, C. A. Manuscript in preparation.